



Verification Mirage: Mapping the Reliability Boundary of Self-Verification in Medical VQA

Ruinan Jin¹², Beidi Zhao¹², Myeongkyun Kang¹², Qiong Zhang³, Xiaoxiao Li¹²

¹The University of British Columbia, ²Vector Institute, ³Redmin University of China

Self-verification, re-invoking the same vision language model (VLM) with identical parameters but in a fresh, independent context to check its own generated answer, is increasingly treated as a default safety layer for medical visual question answering (VQA). We argue this practice is fundamentally unreliable. We introduce **VeriMap**, a diagnostic framework that maps the reliability boundary of medical VLM self-verification. It decomposes verifier behavior along two axes: *discrimination capability* and *agreement bias*. In self-verification, the verifier and the answer generator are capacity-coupled, so the verifier overly agrees with the generator, sustaining a high appearance of accuracy for the generator. We call this a **verification mirage**: a regime where the verifier is simultaneously *high in verifier error and high in agreement bias*, driven by systematic false acceptance of incorrect answers. In this work, evaluating six open-weight VLMs across five medical VQA datasets and seven medical tasks, we reveal that: **(i)** The boundary is task-conditioned. Knowledge-intensive clinical tasks sit deepest in the mirage, and simpler tasks are more resistant, with perceptual tasks falling in between. **(ii)** Verification is not an independent safety signal. Our logistic mixed-effects analysis shows verifier error and agreement bias are significantly more likely when the generator errs, and saliency analyses confirm verifiers under-attend to image evidence relative to generators. We call this phenomenon as **lazy verifier**. **(iii)** Cross-verification can reduce verification mirage, though the mirage is not fully eliminated. **(iv)** The failure is amplified rather than corrected when verification is reused: in multi-turn actor-verifier loops, most initially wrong answers are *locked in* by false verification. In this work, our setup uses clean benchmarks, the observed boundary likely *underestimates* failures in real clinical deployment.

1 Introduction

Medical visual question answering (VQA) is one of the highest-stakes applications of vision-language models (VLMs). From chest X-ray report generation (Lovelace and Mortazavi, 2020) to histopathology question answering (Seyfioglu et al., 2024), VLMs are increasingly being considered for clinical and biomedical use. However, a fundamental safety question remains: *how do we know when a VLM’s output is wrong?* Hallucinated findings, misidentified anatomy, incorrect disease labels, and unsupported diagnostic explanations can all become false clinical claims in settings where reliability

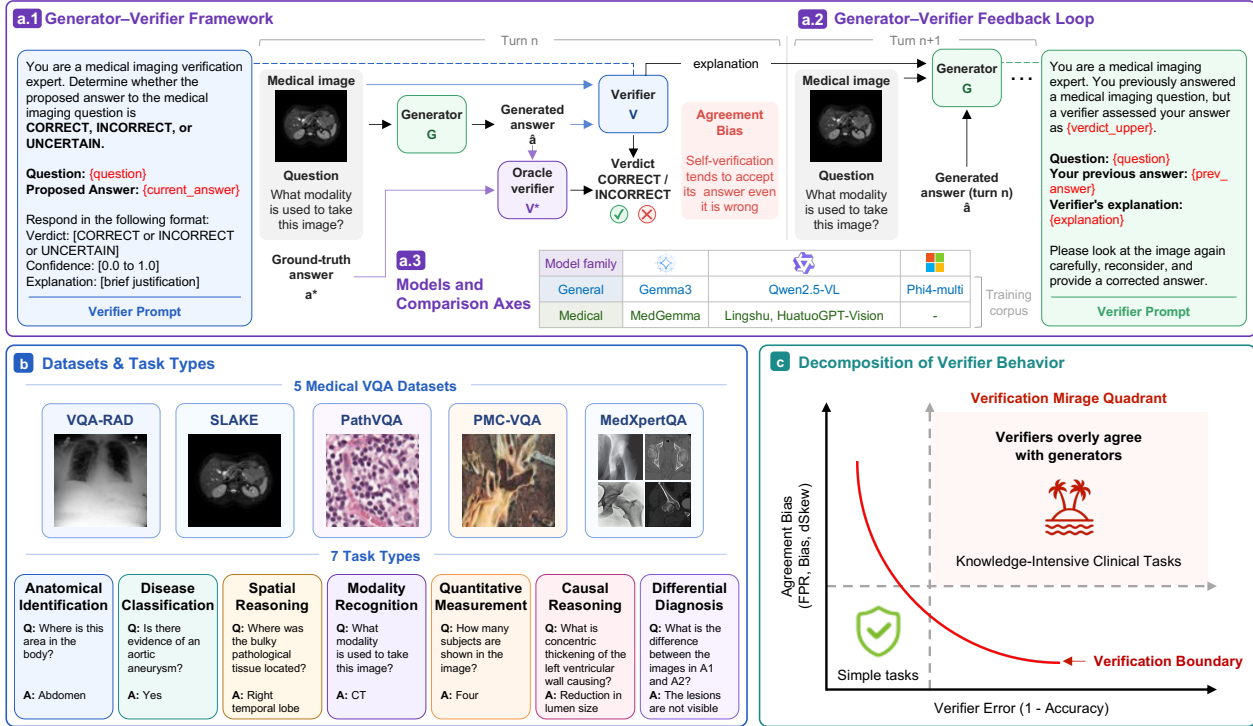


Figure 1 Overall study pipeline. (a) Medical VQA verification is studied through a generator–verifier setup: a generator answers an image–question pair, and a verifier judges the answer against an oracle correctness label. We evaluate both single-turn verification and multi-turn feedback loops, and compare self- and cross-verification across general-domain and medical-domain VLMs. (b) Experiments cover five medical VQA datasets and seven task types, from perceptual recognition to knowledge-intensive clinical reasoning. (c) VeriMap decomposes verifier behavior into discrimination capability and agreement bias, exposing the high-error, high-bias *verification mirage* regime.

is critical.

A natural response is *self-verification*: re-invoking the same VLM, with identical parameters but in an independent context, to check its own generated answer at inference time, as shown in Fig. 1. This strategy is attractive because it is lightweight, requires no additional labeled data or external tools, and integrates directly into existing VLM pipelines. Self-verification has been widely adopted at inference time in VLM tasks (Wu et al., 2025b; Tian et al., 2025; Qian et al., 2026), and even used as a reward signal in reinforcement learning (Liu et al., 2025). In the medical domain, it underlies clinical fact-checking and report verification approaches (Chung et al., 2025; Liu et al., 2024). All of these approaches rely on an implicit promise: even when generation fails, recognition may still succeed (Kadavath et al., 2022; Ren et al., 2023).

We argue that this promise is unreliable in medical VQA tasks, a challenging and high-stakes application field. In self-verification, the verifier and generator share model capacity, training distribution, visual grounding limitations, and medical knowledge boundaries. If the generator fails due to the lack of the relevant visual evidence or clinical knowledge, the verifier may fail for the same reason. Self-verification may therefore become a consistency check over the model’s own answer rather than an independent correctness check.

Existing evaluations are often too coarse to expose this problem. By reporting only a single aggregate verifier-accuracy score over all medical VQA tasks (Xu et al., 2025; Zhong et al., 2025), prior work

implicitly treats medical VQA as a homogeneous problem and conflates two qualitatively different failure modes: failing to *discriminate* correct from incorrect answers, and *over-accepting* whatever the generator proposed. The conflation hides a regime that is uniquely dangerous in medicine: when the verifier and generator share model capacity, the verifier tends to overly agree with the generator’s answer, sustaining the appearance of accuracy while being simultaneously *high in verifier error and high in agreement bias*, driven by systematic false acceptance of incorrect answers. We call this regime the **verification mirage**. The failure is especially dangerous in medicine, where marking an incorrect medical answer as correct can carry direct clinical risk. We therefore ask: *can VLMs be reliable self-verifiers in medical VQA tasks?*

To answer this question, we introduce VeriMap, a diagnostic framework for mapping the reliability boundary of medical VLM self-verification. We operationalize verification as error detection over generated answers and evaluate it across five medical VQA benchmarks and diverse VLMs. Whereas prior evaluations report only a single aggregate verifier-accuracy score over all medical VQA tasks, VeriMap introduces **three complementary novelties**: **(i)** a *task-type decomposition* from perceptual tasks (modality recognition, anatomical identification, spatial cognition) to knowledge-intensive clinical tasks (disease classification, differential diagnosis, causal reasoning), along which generator accuracy itself drops sharply; **(ii)** a *two-axis decomposition of verifier behavior* into **discrimination capability** (verifier accuracy, i.e., the ability to distinguish correct from incorrect answers) and **agreement bias** (the tendency to accept a proposed answer regardless of correctness), instead of a single accuracy number; and **(iii)** a *generator-coupled analysis* that studies how verifier accuracy and verifier agreement bias *covary* with generator accuracy across these categories, pinpointing precisely when the verification mirage emerges, namely the regimes in which the verifier still appears accurate yet disproportionately endorses the generator’s wrong answers.

Our analysis reveals four properties of this reliability boundary. **(i) The mirage is task-conditioned.** Knowledge-intensive clinical tasks (differential diagnosis, causal explanation, disease classification) sit deepest in the mirage quadrant and remain unreliable across all evaluated models, including medical-specialized ones; structured tasks like quantitative measurement are most resistant, while perceptual tasks (modality, anatomy, spatial) span the middle. **(ii) Verifiers are lazy, not independent of generators.** A logistic mixed-effects analysis shows verifier error is significantly more likely when the generator errs, and saliency analyses reveal a **lazy-verifier effect**: verifiers attend less to image evidence than generators do, especially on false positives. **(iii) Cross-verification can reduce verification mirage.** Verification across different model families, training corpora, and parameter scales can lower agreement bias and verification error, even though the mirage is not fully eliminated. **(iv) Errors compound rather than self-correct.** In multi-turn actor-verifier loops, false verification *locks in* initially wrong answers, turning isolated verifier mistakes into system-level failures. Our findings highlight that medical VLM self-verification cannot serve as a universal safety layer. The central question is not whether a model agrees with its own answer, but whether it can detect when that answer is wrong.

2 Related Work

Reliability and verification of medical VLMs. Medical VLMs raise distinctive reliability concerns because their errors can produce false clinical claims, including hallucinated findings, misidentified anatomy, incorrect disease labels, or unsupported diagnoses. Prior work has approached this through factuality and grounding tools: phrase-grounded fact-checking for chest X-ray report generation (Mahmood et al., 2025), EHR-grounded verification of LLM-generated clinical text (Chung et al., 2025), retrieval-augmented clinical claim verification (Liu et al., 2024), and uncertainty- or

entropy-based hallucination detection (Liao et al., 2025b). Medical VQA benchmarks (Lau et al., 2018; Liu et al., 2021; He et al., 2020; Zhang et al., 2023; Zuo et al., 2025; Pal et al., 2025; Zhong et al., 2025) provide controlled substrates for evaluation, and recent medical VLMs report aggregate performance on them (Xu et al., 2025; Sellergren et al., 2025).

Self-verification in LLMs and VLMs. Self-verification, using a model to check its own output, has emerged as a lightweight inference-time mechanism for filtering or correcting errors, motivated by the hypothesis that judging a candidate answer may be easier than generating one from scratch (Kadavath et al., 2022; Ren et al., 2023; Weng et al., 2023; Manakul et al., 2023). The same intuition has been transferred to code generation (Ni et al., 2023; Chen et al., 2023), multimodal reasoning (Sun et al., 2025; Wang et al., 2025), and to vision-language models Andrade et al. (2025), where self-verification or retrospective resampling is used to suppress hallucinations and improve generation (Wu et al., 2025b; Tian et al., 2025; Qian et al., 2026; Liao et al., 2025a; Wu et al., 2025a). Self-verification has further been adopted as a learned signal: process reward models judge intermediate reasoning steps (Wang et al., 2025; Zhang et al., 2025), and reinforcement learning frameworks use the model’s own verification as a reward (Liu et al., 2025). Across this literature, verification is treated as a *means to an end* and evaluated through downstream task accuracy, not as an object of study; whether the verification signal itself is reliable, and under what conditions, is left implicit.

Verifier biases and reliability. A growing body of work shows that self-verification is not an unbiased safety signal (Xu et al., 2024; Andrade et al., 2025; Wang et al., 2026; Panickssery et al., 2024; Wataoka et al., 2024). Xu et al. (2024) report that LLMs systematically prefer and amplify their own outputs during self-refinement, a self-preference bias that can compound rather than correct errors. (Andrade et al., 2025) formalize *agreement bias* in MLLM verification: verifiers over-validate flawed candidate trajectories and exhibit near-chance true-negative rates when the candidate is wrong. (Wang et al., 2026) attribute a portion of this failure to insufficient visual grounding-verifier scores are confounded by misperceived image evidence, leading to incorrect acceptance even when the textual reasoning is well-formed. These studies establish that verifiers fail in characteristic ways, but they do so on general-domain benchmarks and collapse verification reliability into a single aggregate accuracy or true-negative rate. Crucially, they do not stratify verifier behavior by task difficulty or characterize how it is coupled to the generator’s competence, both of which we show are essential to understanding medical-VQA verification, where generator accuracy varies sharply across task categories.

3 VeriMap: A Novel Protocol for Auditing Self-Verification Reliability

We develop **VeriMap**, a novel protocol for auditing when medical VLM self-verification provides genuine error detection rather than agreement-biased reassurance. **VeriMap** differs from prior verifier evaluations in two ways: **(i)** it decomposes verifier behavior along *two metric axes*: *discrimination capability* and *agreement bias*; and **(ii)** it audits the verifier-generator coupling through generalized mixed-effects model analysis that quantifies inherited blind spots. The remainder of this section formalizes each component and defines the experimental settings used to instantiate them.

3.1 Problem Formulation

Setup. As shown in Fig. 1(a), each query example is a tuple (I, q, a^*, k) comprising a medical image I , a question q , a ground-truth answer a^* , and a medical VQA task label $k \in \mathcal{K}$. A generator VLM G produces $\hat{a} = G(I, q)$. An oracle verifier V^* assigns an oracle correctness label $y^* = C(\hat{a}, a^*) \in \{0, 1\}$ via an answer-correctness function C . A VLM verifier V then receives (I, q, \hat{a}) and outputs a verdict $v \in \{\text{CORRECT}, \text{INCORRECT}, \text{UNCERTAIN}\}$, which we convert into a predicted correctness label $\hat{y} = \mathbb{1}[v = \text{CORRECT}]$. We use the star superscript (\star) for oracle quantities (e.g., a^*, V^*, y^*) and the hat ($\hat{\cdot}$) for VLM-produced quantities (e.g., \hat{a}, \hat{y}), so the symbol immediately conveys oracle vs. predicted.

3.2 Medical VQA Task Taxonomy

Seven tasks. We label each example with one of seven tasks \mathcal{K} : *modality recognition, anatomical identification, disease classification, spatial localization, quantitative measurement, differential diagnosis, and causal explanation*, capturing the main verification demands surfaced in prior medical VQA and clinical reasoning work (Lau et al., 2018; Liu et al., 2021; He et al., 2021; Zhang et al., 2023; Chen et al., 2024b; Zuo et al., 2025). To make the task-type dimension well-defined, each task we adopt here corresponds to a distinct visual or clinical evidence demand and the tasks admit a partial ordering from perceptual (modality, anatomy, spatial) to knowledge-intensive clinical tasks (disease, differential, causal), reflecting the depth of medical knowledge required. Each task label has a consistent semantics across all five medical VQA benchmarks, so the same definition applies regardless of source dataset.

Labeling and validation. We assign k by majority vote across GPT-5.4, Gemini 2.5-flash, and Qwen3 prompted with the same taxonomy and output schema; ties or invalid outputs are manually adjudicated. We validate the labels on a manually annotated subset, reporting inter-LLM agreement rate, full prompts, voting rules, and per-task confusion are in Appendix A. The subset of the task labels is further validated by human.

3.3 Two-Axis Decomposition of Verifier Behavior

Unlike prior verifier evaluations that collapse verifier behavior into a single accuracy metric, VeriMap disentangles two dimensions of verifier behavior: (1) *discrimination capability*, *i.e.* whether the verifier correctly identifies errors, and (2) *agreement bias*, *i.e.* whether the verifier tends to endorse the presented answer regardless of its correctness.

Discrimination capability. The ability to distinguish correct from incorrect answers, captured by verifier accuracy $\text{Acc} = \Pr(\hat{y} = y^*)$.

Agreement bias. The tendency to deviate from the oracle in a directional way, over-accepting wrong answers or over-rejecting correct ones, captured by the false-positive rate $\text{FPR} = \Pr(\hat{y} = 1 \mid y^* = 0)$, and, following prior work on agreement bias (Andrade et al., 2025; Xu et al., 2024), we also use bias $\text{Bias} = \frac{1}{n} \sum_{i=1}^n d_i = \frac{\text{FP-FN}}{N}$ and dSkew $\text{dSkew} = 1 - \frac{\sum_{i,j} |d_i - d_j|}{\sum_{i,j} |d_i + d_j|}$, where $d_i = \hat{y}_i - y_i^* \in \{-1, 0, +1\}$. Positive bias and dSkew indicate systematic over-acceptance relative to the oracle verifier.

Verification boundary defined by the two axes. A verifier can occupy any quadrant of the discrimination–bias plane: *low verifier error, low bias* (the desired regime); *low verifier error, high bias* (often correct but accepts borderline wrong answers); *high verifier error, low bias* (random or refusing); or *high verifier error, high bias*—the verification mirage.

3.4 Statistical Testing of Verifier-Generator Coupling

We use linear and logistic mixed-effects models to quantify generator–verifier coupling while accounting for the hierarchical structure of the data. Since verifier correctness is binary at the sample level, we employ logistic mixed-effects models (GLMMs) with a logit link (Bolker et al., 2009; Faraway, 2016), which appropriately model binary outcomes and yield interpretable odds ratios. For aggregated cell-level metrics (e.g., FPR, Bias, and dSkew), we instead use linear mixed-effects models (LMMs) (Bates et al., 2015). In both cases, observations are nested within task categories, models, and datasets, motivating a mixed-effects formulation rather than fixed-effects-only regression. Random intercepts capture differences in baseline verifier behavior across groups, while random slopes allow the strength of generator-verifier coupling itself to vary across task categories, models, and datasets. This directly tests whether some settings exhibit systematically stronger or weaker dependence of verifier errors on generator errors. Model significance and interaction effects are assessed through likelihood-ratio tests between nested models fit by maximum likelihood, enabling formal evaluation of both the existence of coupling and the heterogeneity of that coupling across groups. Full model specifications, estimation details, sample sizes, likelihood-ratio statistics, and goodness-of-fit metrics are provided in Appendix D. For pairwise comparisons involving grounding and loop interventions, where normality assumptions may not hold, we use paired non-parametric tests.

4 Mapping the Verification Mirage

4.1 Datasets and Models

Datasets. We use five publicly available medical VQA datasets: VQA-RAD (Lau et al., 2018), PathVQA (He et al., 2020), SLAKE (Liu et al., 2021), PMC-VQA (Zhang et al., 2023), and MedXpertQA (Zuo et al., 2025), all normalized to the schema (I, q, a^*, k) .

Models. We evaluate six open-weight, instruction-tuned VLMs spanning general-domain and medical-specialized backbones: *Qwen2.5-VL-7B-Instruct* (Yang et al., 2025), *Gemma-3* (Team, 2025), *Phi-4-Multimodal-Instruct* (Abouelenin et al., 2025), *MedGemma* (Selligren et al., 2025), *HuatuoGPT-Vision* (Chen et al., 2024a), and *Lingshu* (Xu et al., 2025). All models share the same image-question-answer interface and verification prompt.

4.2 Verification Boundary on Verifiers Discrimination Capability and Agreement Bias

We instantiate the discrimination-bias plane defined in §3.3 by plotting verifier error ($1 - \text{Acc}$) against each of the three agreement-bias metrics. Fig. 2 shows the empirical occupancy: each point is one $\langle \text{task}, \text{VLM} \rangle$ cell ($7 \text{ tasks} \times 6 \text{ models} = 42 \text{ points per panel}$), with task encoded by color and model by marker shape.

Most tasks fall in the verification mirage quadrant. The vast majority of the 42 $\langle \text{task}, \text{model} \rangle$ measurements concentrate in the upper-right region of all three panels, with verifier error $\geq 40\%$ and agreement bias well above the midpoint of every metric (FPR $\geq 60\%$, Bias $\geq 35\%$, D-Skew $\geq 30\%$). This is the **verification mirage quadrant** identified in §3.3: a verifier that is simultaneously poor at distinguishing correct from incorrect answers and systematically biased toward acceptance. The desired regime (reliable, unbiased self-verification) in the lower-left is essentially empty. Marker shapes within each color cluster show that swapping the underlying VLM shifts the per-task position somewhat but does not move it out of the mirage region for the hardest clinical tasks. Even the most discriminating verifier remains in the high-bias half-plane on differential diagnosis and causal

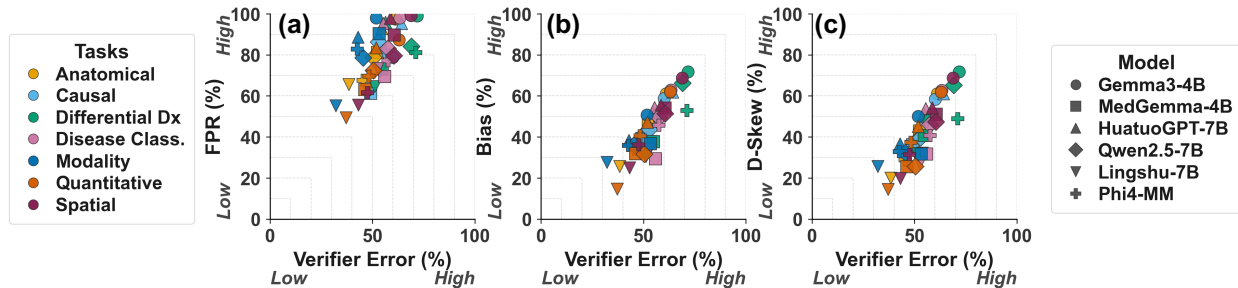


Figure 2 Verification boundary in the discrimination-bias plane. Each panel plots verifier error ($1 - \text{Acc}$, x -axis) against one agreement-bias metric (y -axis): **(a)** FPR, **(b)** Bias, **(c)** D-Skew. Each marker is one $\langle \text{task}, \text{model} \rangle$ measurement; *color* denotes the medical QA task and *marker shape* denotes the VLM. The dashed corner annotations mark the *verification mirage* quadrant (upper right: high verifier error and high agreement bias, introduced in §3.3) and the desired regime (lower left: low error, low bias).

explanation, indicating that no evaluated model crosses the verification boundary on knowledge-intensive clinical tasks.

Discrimination capability and agreement bias rise together. All three panels show a monotonic positive relationship: as verifier error grows, FPR, Bias, and D-Skew rise alongside it. This co-rise is informative, not a definitional artifact. Verifier error $1 - \text{Acc} = (\text{FP} + \text{FN})/N$ pools both false acceptances (FP) and false rejections (FN), so a rising FPR alone is consistent with two scenarios: *(i) symmetric* error growth in which FP and FN climb together, or *(ii) asymmetric* growth in which FP outpaces FN. The Bias and D-Skew panels disambiguate these cases. Because $\text{Bias} = (\text{FP} - \text{FN})/N$ measures the *signed asymmetry* between the two error types, symmetric growth would leave Bias near zero, and growth skewed toward over-rejection would push Bias *down*. The observed positive slope in panels (b) and (c) therefore shows that FP grows faster than FN as the verifier becomes less accurate and verifier mistakes are directionally biased toward false acceptance, the failure mode VeriMap is designed to expose.

Tasks separate along the boundary by clinical-knowledge demand. *Quantitative measurement* (orange) is the only task with multiple cells in the lower-left of the plane (verifier error $\sim 30\text{-}40\%$, FPR $\sim 50\text{-}70\%$): the structured, checkable nature of these questions yields the most-resistant verifier behavior. The knowledge-intensive clinical tasks, such as *differential diagnosis* (green), *causal explanation* (light blue), and *disease classification* (pink), cluster densely in the upper-right mirage quadrant, with several differential-diagnosis cells saturating FPR at $\sim 95\text{-}100\%$. The remaining perceptual tasks (*modality recognition*, *anatomical identification*, *spatial localization*) span the middle of the boundary, exhibiting moderate verifier error but already-substantial agreement bias.

The three agreement-bias metrics tell a consistent story. FPR, Bias, and D-Skew all show the same mirage-quadrant occupancy, the same monotonic trend with verifier error, and the same task ordering. The Bias and D-Skew panels show visually cleaner linear trends because the FPR panel suffers a ceiling effect (many high-error cells already saturate FPR at $\sim 100\%$).

4.3 Verification is Coupled to Generator Failure

The mirage in §4.2 suggests that self-verification is not an independent error signal. We test that hypothesis directly through two complementary lenses: **(i) Error coupling:** does the verifier error whenever the generator errors? and **(ii) Agreement-bias slopes:** does verifier permissiveness rise with generator difficulty?

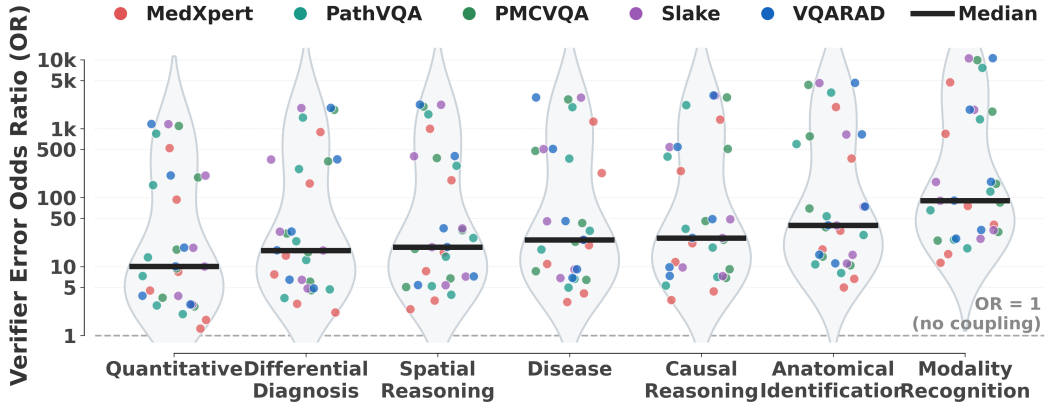


Figure 3 Generator-verifier error coupling by task. Each violin shows the distribution of model- and dataset-conditioned odds ratios (ORs) from a logistic GLMM. Tasks are ordered by median OR; dots denote individual model×dataset cells. OR= 1 indicates no coupling, while larger ORs indicate that verifier errors are more likely when the generator is wrong. Full model specification is provided in Appendix D.1.

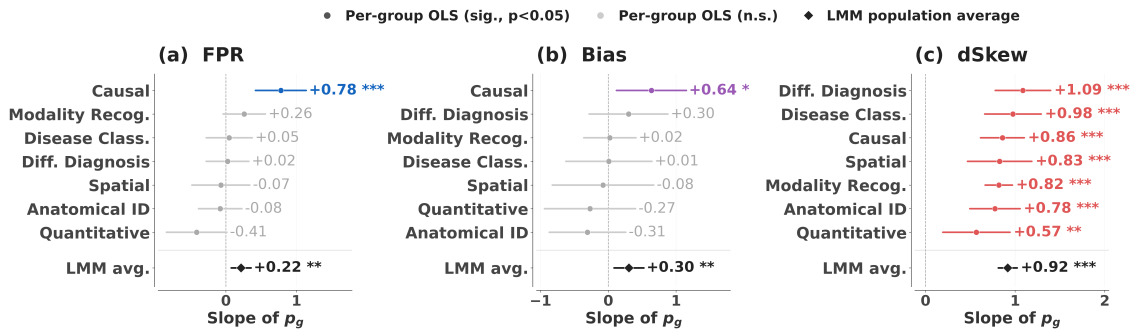


Figure 4 Rows show task-wise OLS slopes of generator error rate $p_g = 1 - \text{Acc}_G$ on each verifier metric, with 95% confidence intervals. Colored points indicate $p < 0.05$; grey points are non-significant. The filled diamond shows the LMM population-average slope. FNR slopes are near zero, while FPR and Bias vary most by task: causal explanation increases most steeply, quantitative measurement is most resistant, and dSkew is positive and significant for all tasks. Full scatter plots and LMM fits are in Appendix B.1.

Verifier errors are strongly coupled to generator errors. As shown in Fig. 3, a generator error increases the predicted probability of a verifier error, corresponding to **57× higher** odds of verifier failure ($p < 0.001$). Likelihood-ratio tests confirm that this coupling varies significantly across groups ($p < 0.001$). *Model identity* is the largest source of variation: the most susceptible model shows coupling nearly **400× stronger** than the most robust one. *Task category* is a secondary but meaningful source: *quantitative measurement* shows the weakest coupling (the verifier retains some independence on a structured, checkable output), while *modality recognition* shows the strongest (the verifier almost always agrees with a wrong generator). *Dataset identity* contributes least, indicating these patterns are not artifacts of any particular benchmark. *Self-verification therefore inherits generator blind spots rather than providing a robust independent safety signal.*

Generator difficulty shifts the verifier from rejection to agreement.

Beyond binary error coupling, we ask whether verifier permissiveness increases as generator perfor-

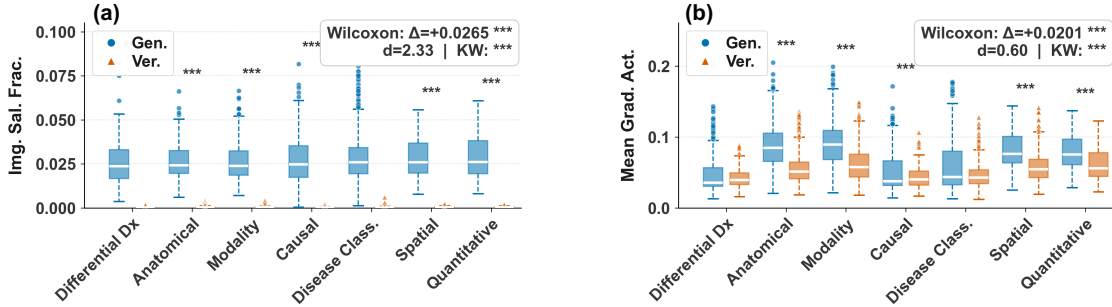


Figure 5 Generator-verifier visual grounding gap. For each paired example, we compare the generator and verifier using two image-grounding proxies: image saliency fraction (**left**) and mean gradient activation (**right**), pooled across five datasets and five models. Boxes show per-task distributions for generators (Gen.) and verifiers (Ver.). Asterisks indicate significant generator > verifier differences within each task category (paired one-sided Wilcoxon, $p < 0.001$). Insets report the overall mean paired difference Δ , Cohen’s d , and a Kruskal–Wallis test across task categories. Verifiers show consistently lower image grounding than generators under both metrics.

mance degrades. In the cell-level LMM (Fig. 4; § 3.4), higher generator error rate $p_g = 1 - \text{Acc}_G$ predicts stronger agreement bias: FPR ($\hat{\beta}_1 = +0.22$, $p = 0.003$), Bias ($\hat{\beta}_1 = +0.31$, $p = 0.008$), and dSkew ($\hat{\beta}_1 = +0.92$, $p < 0.001$) all increase with p_g . In contrast, FNR is flat and non-significant ($\hat{\beta}_1 = -0.04$, $p = 0.54$), suggesting that harder generation makes verifiers more accepting rather than more cautious. The effect is task-dependent: causal explanation shows the steepest significant FPR and Bias slopes, quantitative measurement is most resistant, and dSkew is positive and significant for all seven tasks.

4.4 The Lazy-Verifier Hypothesis: Less Looking, More Agreeing

If verification is to provide an independent safety check, the verifier must ground its judgment in the same image evidence the generator used. We test this directly by comparing image-attention via attention scores and gradient activation scores between the generator and verifier on the same examples (Fig. 5). The qualitative analysis can be found in Appendix B.2.

Verifiers look at the image far less than generators. Verifier image-attention is significantly lower than generator image-attention under both image saliency ($\Delta = +0.027$, Cohen’s $d = 2.33$, $p < 0.001$) and gradient activation ($\Delta = +0.020$, $d = 0.60$, $p < 0.001$).

The size of the gap is task-conditioned. The pattern holds for *every* one of the seven medical VQA tasks, but the gap widens precisely on the tasks that require re-grounding the image, such as spatial reasoning and quantitative measurement.

Lazy looking is a candidate mechanism behind the verification mirage. These results identify a likely mechanism behind the verification mirage of §4.2 and the generator coupling of §4.3: rather than independently re-grounding its decision in the medical image, the verifier behaves as a *textual plausibility checker* on the proposed answer. Note that saliency and gradient analyses are correlational rather than causal; we therefore position VeriMap as a diagnostic framework that surfaces this hypothesis and opens a concrete path for follow-up work.

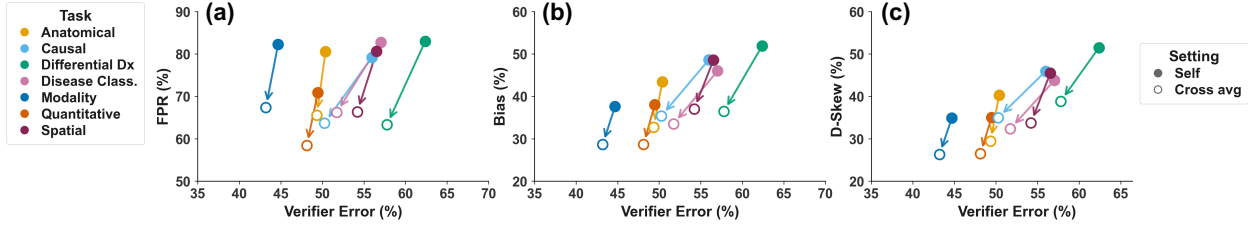


Figure 6 Self-verification and cross-verification averages compared across tasks. Filled markers denote self-verification, hollow markers denote cross-verification averages, and arrows point from self to cross. Cross-verification usually lowers verifier error, FPR, bias, and dSkew, but the gains are task-dependent and remain limited in magnitude.

4.5 Cross-Verification Substantially Can Reduce Agreement Bias and Verification Error

If self-verification fails because the verifier and generator share capacity (§4.3), can we break the coupling by routing verification to a *different* model? We replace $V = G$ with a battery of cross-verifiers spanning other model families, training corpora, and parameter scales, and average the resulting per-task metrics. The result is the *Cross avg* setting in Fig. 6.

Cross-verification shifts every task toward the desired regime. For all seven tasks, the Cross-avg point sits lower-left of its Self counterpart in all three panels: agreement bias and verifier error *both* decrease when the verifier is no longer the generator. The largest gains are on the hardest task. *Differential diagnosis* (green) shows the largest Self-to-Cross-avg shift in all three panels, and the other knowledge-intensive clinical tasks (*causal explanation*, *disease classification*) also gain substantially. *Quantitative measurement* (orange) starts closest to the desired regime under self-verification and accordingly has the smallest absolute shift.

Agreement bias drops more than discrimination error. The dominant component of the shift is downward (lower agreement bias) rather than leftward (lower verifier error): FPR drops by roughly $\sim 12\text{--}20\%$ across tasks, while verifier error drops only $\sim 2\text{--}5\%$. Bias and D-Skew show the same pattern. Cross-verification therefore primarily reduces *agreement* between verifier and generator, with a smaller secondary improvement in raw discrimination.

Takeaway. Cross-family, cross-corpus, and cross-size verification, averaged together as Cross avg, is a potential mitigation method we identify: it can loosen the coupling and reduce agreement bias across all seven tasks, which delivers the largest gains precisely where self-verification fails worst (knowledge-intensive tasks). However, agreement bias is partially mitigated via cross-verifier, not simply removed.

Appendix B.3 and B.4 further isolate the effect of using the medical (domain-expert model) verifier and the same-family verifier scaling.

4.6 Errors Compound Rather Than Self-Correct in Multi-Turn Loops

What if self-verification is not used just once, but *reused* as a feedback signal in actor-verifier loops? We feed each turn’s verdict and explanation back to the generator, which revises its answer, and track the fate of initially wrong answers across four revision turns (Fig. 7). This tests whether reusing self-verification *corrects* verifier mistakes or amplifies them into system-level failures.

Wrong answers lock in rather than self-correct. Only 2.2–3.8% of initially wrong answers are cor-

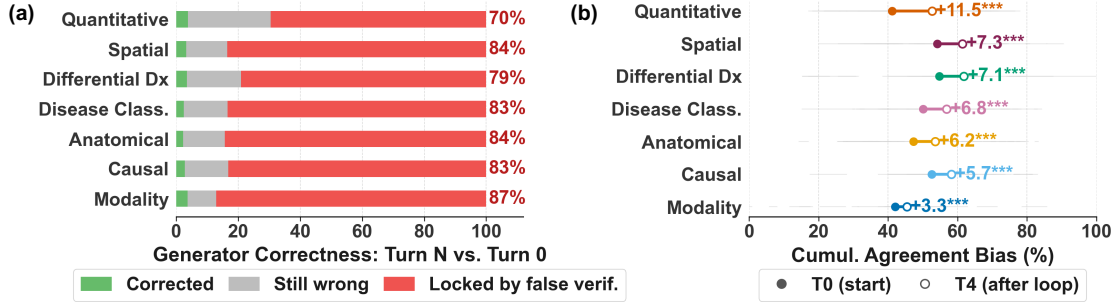


Figure 7 Verifier-generator feedback loop. (a) Generator side: fate of answers that are wrong at Turn 0 after four verification–revision turns. **Corrected** means the final answer becomes oracle-correct; **still wrong** means the final answer remains incorrect and is not verified as correct; **locked by false verification** means the final answer remains incorrect but is verified as correct. Red numbers show the locked rate. **(b) Verifier side:** cumulative agreement bias at Turn 0 versus Turn 4. Filled circles denote T0, open circles denote T4, gray stubs denote model×dataset cells, and annotations show mean percentage-point increases. All tasks increase significantly (** $p < 0.001$, one-sided Wilcoxon signed-rank test).

rected over four turns, while 69.5%–87.1% are *locked in* by false verification (quantitative measurement at the low end; the other six tasks above 79%; Fig. 7a). In other words, when self-verification is reused in multi-turn actor-verifier loops, false verification **locks in** initially wrong answers rather than correcting them, amplifying isolated verifier mistakes into system-level failures.

Accumulation preserves the task-conditioned boundary. Cumulative agreement bias rises significantly from turn 0 to turn 4 for all seven tasks (one-sided Wilcoxon signed-rank, $n=25$ pairs/task, all $p < 0.001$; Fig. 7b), with the largest increases on quantitative measurement (+11.5 %), spatial reasoning (+7.3 %), differential diagnosis (+7.1 %), and disease classification (+6.8 %); modality recognition grows least (+3.3 %). The loop does not erase the earlier reliability boundary. It preserves the same task hierarchy and accumulates the most false acceptance precisely on the tasks that were already hardest to verify. Appendix B.5 further complements Fig. 7 from a turn-wise perspective.

5 Conclusion

We introduced **VeriMap**, a diagnostic framework that audits medical VLM self-verification along two axes: *discrimination capability* and *agreement bias*, and exposes when self-verification produces a **verification mirage**: high apparent accuracy that masks systematic over-acceptance on generators (high agreement bias) where the verifier is simultaneously high in error. Three properties of this mirage stand out. It is *task-conditioned*: verifier reliability collapses on knowledge-intensive clinical tasks (differential diagnosis, causal explanation, disease classification) while remaining tolerable on perceptual tasks. It is *generator-coupled*: the verifier inherits the generator’s blind spots and behaves as a **lazy verifier** that under-attends to image evidence, making self-verification more a consistency check than an independent audit. And it is *amplified by reuse*: in multi-turn actor-verifier loops, false verification **locks in** initially wrong answers rather than correcting them. On the positive side, **VeriMap** also identifies a practical mitigation: *cross-verification* can reduce verification mirage although not fully mitigate it. The takeaway is therefore not that self-verification is unusable, but that it is *conditional*: a useful safety layer when its boundary is mapped, audited, and respected. Reliable deployment requires explicit reporting of both verification errors and agreement bias. The right question, then, is not whether a medical VLM agrees with its own answer, but whether it can

detect when that answer is wrong.

References

- Abdelrahman Abouelenin, Atabak Ashfaq, Adam Atkinson, Hany Awadalla, Nguyen Bach, Jianmin Bao, Alon Benhaim, Martin Cai, Vishrav Chaudhary, Congcong Chen, et al. Phi-4-mini technical report: Compact yet powerful multimodal language models via mixture-of-loras. *arXiv preprint arXiv:2503.01743*, 2025.
- Moises Andrade, Joonhyuk Cha, Brandon Ho, Vriksha Srihari, Karmesh Yadav, and Zsolt Kira. Let’s think in two steps: Mitigating agreement bias in mllms with self-grounded verification. *arXiv preprint arXiv:2507.11662*, 2025.
- Douglas Bates, Martin Mächler, Ben Bolker, and Steve Walker. Fitting linear mixed-effects models using lme4. *Journal of statistical software*, 67:1–48, 2015.
- Benjamin M Bolker, Mollie E Brooks, Connie J Clark, Shane W Geange, John R Poulsen, M Henry H Stevens, and Jada-Simone S White. Generalized linear mixed models: a practical guide for ecology and evolution. *Trends in ecology & evolution*, 24(3):127–135, 2009.
- Junying Chen, Chi Gui, Ruyi Ouyang, Anningzhe Gao, Shunian Chen, Guiming Hardy Chen, Xidong Wang, Zhenyang Cai, Ke Ji, Xiang Wan, et al. Towards injecting medical visual knowledge into multimodal llms at scale. In *Proceedings of the 2024 conference on empirical methods in natural language processing*, pages 7346–7370, 2024a.
- Pengcheng Chen, Jin Ye, Guoan Wang, Yanjun Li, Zhongying Deng, Wei Li, Tianbin Li, Haodong Duan, Ziyang Huang, Yanzhou Su, et al. Gmai-mmbench: A comprehensive multimodal evaluation benchmark towards general medical ai. *Advances in Neural Information Processing Systems*, 37:94327–94427, 2024b.
- Xinyun Chen, Maxwell Lin, Nathanael Schärli, and Denny Zhou. Teaching large language models to self-debug. *arXiv preprint arXiv:2304.05128*, 2023.
- Philip Chung, Akshay Swaminathan, Alex J Goodell, Yeasul Kim, S Momsen Reincke, Lichy Han, Ben Deverett, Mohammad Amin Sadeghi, Abdel-Badiah Ariss, Marc Ghanem, et al. Verifact: Verifying facts in llm-generated clinical text with electronic health records. *arXiv preprint arXiv:2501.16672*, 2025.
- Julian J Faraway. *Extending the linear model with R: generalized linear, mixed effects and nonparametric regression models*. Chapman and Hall/CRC, 2016.
- Xuehai He, Yichen Zhang, Luntian Mou, Eric Xing, and Pengtao Xie. Pathvqa: 30000+ questions for medical visual question answering. *arXiv preprint arXiv:2003.10286*, 2020.
- Xuehai He, Zhuo Cai, Wenlan Wei, Yichen Zhang, Luntian Mou, Eric Xing, and Pengtao Xie. Towards visual question answering on pathology images. In *Proceedings of the 59th Annual Meeting of the Association for Computational Linguistics and the 11th International Joint Conference on Natural Language Processing (Volume 2: Short Papers)*, pages 708–718, 2021.
- Saurav Kadavath, Tom Conerly, Amanda Askell, Tom Henighan, Dawn Drain, Ethan Perez, Nicholas Schiefer, Zac Hatfield-Dodds, Nova DasSarma, Eli Tran-Johnson, et al. Language models (mostly) know what they know. *arXiv preprint arXiv:2207.05221*, 2022.
- Jason J Lau, Soumya Gayen, Asma Ben Abacha, and Dina Demner-Fushman. A dataset of clinically generated visual questions and answers about radiology images. *Scientific data*, 5(1):180251, 2018.
- Yuan-Hong Liao, Rafid Mahmood, Sanja Fidler, and David Acuna. Can large vision-language models correct semantic grounding errors by themselves? In *Proceedings of the Computer Vision and Pattern Recognition Conference*, pages 14667–14678, 2025a.
- Zehui Liao, Shishuai Hu, Ke Zou, Mengyuan Jin, Yanning Zhang, Huazhu Fu, Liangli Zhen, and Yong Xia. Univrse: Unified vision-conditioned response semantic entropy for hallucination detection in medical vision-language models. *arXiv preprint arXiv:2503.20504*, 2025b.

- Bo Liu, Li-Ming Zhan, Li Xu, Lin Ma, Yan Yang, and Xiao-Ming Wu. Slake: A semantically-labeled knowledge-enhanced dataset for medical visual question answering. In *2021 IEEE 18th international symposium on biomedical imaging (ISBI)*, pages 1650–1654. IEEE, 2021.
- Hao Liu, Ali Soroush, Jordan G Nestor, Elizabeth Park, Betina Idnay, Yilu Fang, Jane Pan, Stan Liao, Marguerite Bernard, Yifan Peng, et al. Retrieval augmented scientific claim verification. *JAMIA open*, 7(1):ooae021, 2024.
- Xiaoyuan Liu, Tian Liang, Zhiwei He, Jiahao Xu, Wenxuan Wang, Pinjia He, Zhaopeng Tu, Haitao Mi, and Dong Yu. Trust, but verify: A self-verification approach to reinforcement learning with verifiable rewards. *arXiv preprint arXiv:2505.13445*, 2025.
- Justin Lovelace and Bobak Mortazavi. Learning to generate clinically coherent chest x-ray reports. In *Findings of the association for computational linguistics: EMNLP 2020*, pages 1235–1243, 2020.
- Razi Mahmood, Diego Machado-Reyes, Joy Wu, Parisa Kaviani, Ken CL Wong, Niharika D’Souza, Manudeep Kalra, Ge Wang, Pingkun Yan, and Tanveer Syeda-Mahmood. Phrase-grounded fact-checking for automatically generated chest x-ray reports. In *International Conference on Medical Image Computing and Computer-Assisted Intervention*, pages 441–452. Springer, 2025.
- Potsawee Manakul, Adian Liusie, and Mark Gales. Selfcheckgpt: Zero-resource black-box hallucination detection for generative large language models. In *Proceedings of the 2023 conference on empirical methods in natural language processing*, pages 9004–9017, 2023.
- Daniel McFadden. Conditional logit analysis of qualitative choice behavior. 1972.
- Shinichi Nakagawa and Holger Schielzeth. A general and simple method for obtaining r^2 from generalized linear mixed-effects models. *Methods in ecology and evolution*, 4(2):133–142, 2013.
- Ansong Ni, Srini Iyer, Dragomir Radev, Veselin Stoyanov, Wen-tau Yih, Sida Wang, and Xi Victoria Lin. Lever: Learning to verify language-to-code generation with execution. In *International Conference on Machine Learning*, pages 26106–26128. PMLR, 2023.
- Ankit Pal, Jung-Oh Lee, Xiaoman Zhang, Malaikannan Sankarasubbu, Seunghyeon Roh, Won Jung Kim, Meesun Lee, and Pranav Rajpurkar. Rexvqa: A large-scale visual question answering benchmark for generalist chest x-ray understanding. In *Biocomputing 2026: Proceedings of the Pacific Symposium*, pages 251–264. World Scientific, 2025.
- Arjun Panickssery, Samuel R Bowman, and Shi Feng. Llm evaluators recognize and favor their own generations. *Advances in Neural Information Processing Systems*, 37:68772–68802, 2024.
- Michael JD Powell et al. The bobyqa algorithm for bound constrained optimization without derivatives. *Cambridge NA Report NA2009/06, University of Cambridge, Cambridge*, 26(26-46):1, 2009.
- Zhe Qian, Nianbing Su, Zhonghua Wang, Hebei Li, Zhongxing Xu, Yueying Li, Fei Luo, Zhuohan Ouyang, and Yanbiao Ma. Svsvr: A self-verification and self-rectification paradigm for multimodal reasoning. *arXiv preprint arXiv:2604.10228*, 2026.
- Jie Ren, Yao Zhao, Tu Vu, Peter J Liu, and Balaji Lakshminarayanan. Self-evaluation improves selective generation in large language models. In *Proceedings on*, pages 49–64. PMLR, 2023.
- Franklin E Satterthwaite. An approximate distribution of estimates of variance components. *Biometrics bulletin*, 2(6):110–114, 1946.
- Andrew Sellergren, Sahar Kazemzadeh, Tiam Jaroensri, Atilla Kiraly, Madeleine Traverse, Timo Kohlberger, Shawn Xu, Fayaz Jamil, Cian Hughes, Charles Lau, et al. Medgemma technical report. *arXiv preprint arXiv:2507.05201*, 2025.
- Mehmet Saygin Seyfioglu, Wisdom O Ikezogwo, Fatemeh Ghezloo, Ranjay Krishna, and Linda Shapiro. Quilt-llava: Visual instruction tuning by extracting localized narratives from open-source histopathology videos. In *Proceedings of the IEEE/CVF Conference on Computer Vision and Pattern Recognition*, pages 13183–13192, 2024.

- Linzhuang Sun, Hao Liang, Jingxuan Wei, Bihui Yu, Tianpeng Li, Fan Yang, Zenan Zhou, and Wentao Zhang. Mm-verify: Enhancing multimodal reasoning with chain-of-thought verification. In *Proceedings of the 63rd Annual Meeting of the Association for Computational Linguistics (Volume 1: Long Papers)*, pages 14100–14115, 2025.
- Gemma Team. Gemma 3 technical report. *CoRR*, abs/2503.19786, 2025. doi: 10.48550/ARXIV.2503.19786. URL <https://doi.org/10.48550/arXiv.2503.19786>.
- Rui Tian, Mingfei Gao, Mingze Xu, Jiaming Hu, Jiasen Lu, Zuxuan Wu, Yinfei Yang, and Afshin Dehghan. Unigen: Enhanced training & test-time strategies for unified multimodal understanding and generation. *arXiv preprint arXiv:2505.14682*, 2025.
- Junxin Wang, Dai Guan, Weijie Qiu, Zhihang Li, Yongbo Gai, Zhengyi Yang, Mengyu Zhou, Erchao Zhao, Xiaoxi Jiang, and Guanjun Jiang. Grounding the score: Explicit visual premise verification for reliable vision-language process reward models. *arXiv preprint arXiv:2603.16253*, 2026.
- Weiyun Wang, Zhangwei Gao, Lianjie Chen, Zhe Chen, Jinguo Zhu, Xiangyu Zhao, Yangzhou Liu, Yue Cao, Shenglong Ye, Xizhou Zhu, et al. Visualprm: An effective process reward model for multimodal reasoning. *arXiv preprint arXiv:2503.10291*, 2025.
- Koki Wataoka, Tsubasa Takahashi, and Ryokan Ri. Self-preference bias in llm-as-a-judge. *arXiv preprint arXiv:2410.21819*, 2024.
- Yixuan Weng, Minjun Zhu, Fei Xia, Bin Li, Shizhu He, Shengping Liu, Bin Sun, Kang Liu, and Jun Zhao. Large language models are better reasoners with self-verification. In *Findings of the Association for Computational Linguistics: EMNLP 2023*, pages 2550–2575, 2023.
- Mingyuan Wu, Meitang Li, Jingcheng Yang, Jize Jiang, Kaizhuo Yan, Zhaoheng Li, Hanchao Yu, Minjia Zhang, and Klara Nahrstedt. Aha moment revisited: Are vlms truly capable of self verification in inference-time scaling? *arXiv preprint arXiv:2506.17417*, 2025a.
- Tsung-Han Wu, Heekyung Lee, Jiabin Ge, Joseph E Gonzalez, Trevor Darrell, and David M Chan. Generate, but verify: Reducing hallucination in vision-language models with retrospective resampling. *arXiv preprint arXiv:2504.13169*, 2025b.
- Weiwen Xu, Hou Pong Chan, Long Li, Mahani Aljunied, Ruifeng Yuan, Jianyu Wang, Chenghao Xiao, Guizhen Chen, Chaoqun Liu, Zhaodonghui Li, et al. Lingshu: A generalist foundation model for unified multimodal medical understanding and reasoning. *arXiv preprint arXiv:2506.07044*, 2025.
- Wenda Xu, Guanglei Zhu, Xuandong Zhao, Liangming Pan, Lei Li, and William Wang. Pride and prejudice: Llm amplifies self-bias in self-refinement. In *Proceedings of the 62nd Annual Meeting of the Association for Computational Linguistics (Volume 1: Long Papers)*, pages 15474–15492, 2024.
- An Yang, Anfeng Li, Baosong Yang, Beichen Zhang, Binyuan Hui, Bo Zheng, Bowen Yu, Chang Gao, Chengen Huang, Chenxu Lv, et al. Qwen3 technical report. *arXiv preprint arXiv:2505.09388*, 2025.
- Xiaoman Zhang, Chaoyi Wu, Ziheng Zhao, Weixiong Lin, Ya Zhang, Yanfeng Wang, and Weidi Xie. Pmc-vqa: Visual instruction tuning for medical visual question answering. *arXiv preprint arXiv:2305.10415*, 2023.
- Xinchen Zhang, Xiaoying Zhang, Youbin Wu, Yanbin Cao, Renrui Zhang, Ruihang Chu, Ling Yang, and Yujiu Yang. Generative universal verifier as multimodal meta-reasoner. *arXiv preprint arXiv:2510.13804*, 2025.
- Yuan Zhong, Ruinan Jin, Qi Dou, and Xiaoxiao Li. Can generalist vision language models (vlms) rival specialist medical vlms? benchmarking and strategic insights. *arXiv preprint arXiv:2506.17337*, 2025.
- Yuxin Zuo, Shang Qu, Yifei Li, Zhangren Chen, Xuekai Zhu, Ermo Hua, Kaiyan Zhang, Ning Ding, and Bowen Zhou. Medxpertqa: Benchmarking expert-level medical reasoning and understanding. *arXiv preprint arXiv:2501.18362*, 2025.

Appendix

A Task Label Construction and Implementation Details

We have visualized the example QA pairs of different reasoning types in Fig. 1.

Each medical VQA sample is assigned to one of seven mutually exclusive reasoning categories: *modality recognition*, *anatomical identification*, *disease classification*, *spatial reasoning*, *causal reasoning*, *differential diagnosis*, and *quantitative measurement*. For datasets without native reasoning annotations, we obtain three independent LLM labels per question and consolidate them into a single label by deterministic majority vote.

Task definitions. *Modality recognition* covers questions about the imaging modality or acquisition type. *Anatomical identification* covers questions about the depicted organ, structure, or anatomical region. *Disease classification* covers questions about the presence of a pathology, finding, or diagnostic category. *Spatial reasoning* covers questions involving location, orientation, laterality, or relative position. *Causal reasoning* covers questions that connect imaging evidence to an underlying mechanism, cause, or clinical implication. *Differential diagnosis* covers questions that distinguish among multiple plausible conditions. *Quantitative measurement* covers questions that require counting, size estimation, or other numeric judgment.

Voting rule. For each sample, we collect one label from each annotator. If at least two annotators agree, we keep the majority label. If all three annotators disagree, we apply the same deterministic tie-breaking rule as the release script and select the alphabetically first label among the three candidates. This procedure provides reproducible labels even under fully split votes.

Oracle judge We instantiate the oracle correctness function $C(\hat{a}, a^*)$ with Gemini-2.5-Flash as an external binary semantic judge. For each generated answer, the judge is given the question q , reference answer a^* , and model answer \hat{a} , and is instructed to return only CORRECT or INCORRECT. We set $C(\hat{a}, a^*) = 1$ only when the judge returns CORRECT, i.e., when \hat{a} semantically matches a^* ; otherwise $C(\hat{a}, a^*) = 0$. The judge accepts clear synonyms and equivalent medical phrasing, but applies strict matching for yes/no questions and assigns no partial credit. Thus, oracle correctness is based on binary semantic equivalence rather than exact string match or lexical-overlap metrics.

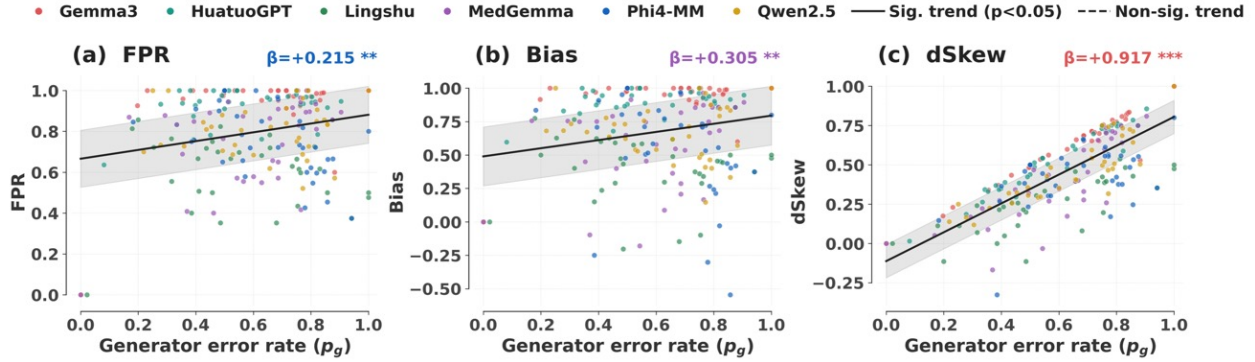


Figure B1 Effect of generator error rate on verifier agreement bias metrics (cell-level scatter). Each panel shows one verifier metric plotted against the generator error rate $p_g = 1 - \text{acc}$ across all 210 cells (7 tasks \times 6 models \times 5 datasets). Points are colored by model. The line shows the LMM fixed-effect slope (solid: $p < 0.05$; dashed: $p \geq 0.05$) and the shaded band is a $\pm 1.96 \times \text{SE}$ uncertainty region. FNR is flat, while FPR and Bias rise significantly with p_g , indicating that generator difficulty makes the verifier more permissive rather than more critical. dSkew shows the strongest and most consistent trend, partly reflecting the algebraic dependence of dSkew on p_g .

B Additional Results

B.1 Higher Generator Error Leads to Higher Verifier Agreement Bias

Fig. B1 provides the cell-level scatter underlying the per-task slope summary in Fig. 4. Each point corresponds to one reasoning type-model-dataset cell, and the fitted line shows the population-average LMM relationship between generator error rate $p_g = 1 - \text{Acc}_G$ and each verifier metric. The figure shows that verifier agreement bias increases as generator difficulty rises: FPR, Bias, and dSkew all exhibit positive trends with p_g , whereas FNR remains comparatively flat in the corresponding analysis. This pattern indicates that harder generator regimes do not make the verifier more cautious; instead, they make the verifier more permissive, increasing its tendency to accept incorrectly generated answers. The cell-level view therefore, supports the main finding in Fig. 4: self-verification is coupled to generator difficulty, and the verifier becomes most agreement-biased precisely in the regimes where the generator is more likely to be wrong.

B.2 Qualitative Analysis of Lazy Verifier

Fig. B2 complements the aggregate grounding analysis by showing representative examples of the **lazy verifier** effect. In both cases, the generator retains meaningful visual grounding. Its patch-level gradient heatmaps contain stronger activations over relevant image regions, and its image-token saliency shows clear peaks. The verifier, however, largely stops looking at the image. Its gradient maps are substantially darker and less spatially informative, while its image-token saliency is close to zero even though the verification task explicitly requires judging whether the answer is supported by the medical image. This contrast suggests that self-verification does not provide an independent visual check. Instead, the verifier often treats the proposed answer as a textual claim to be accepted or rejected using language-side plausibility, which helps explain the high false-positive rate and agreement bias observed in the main results.

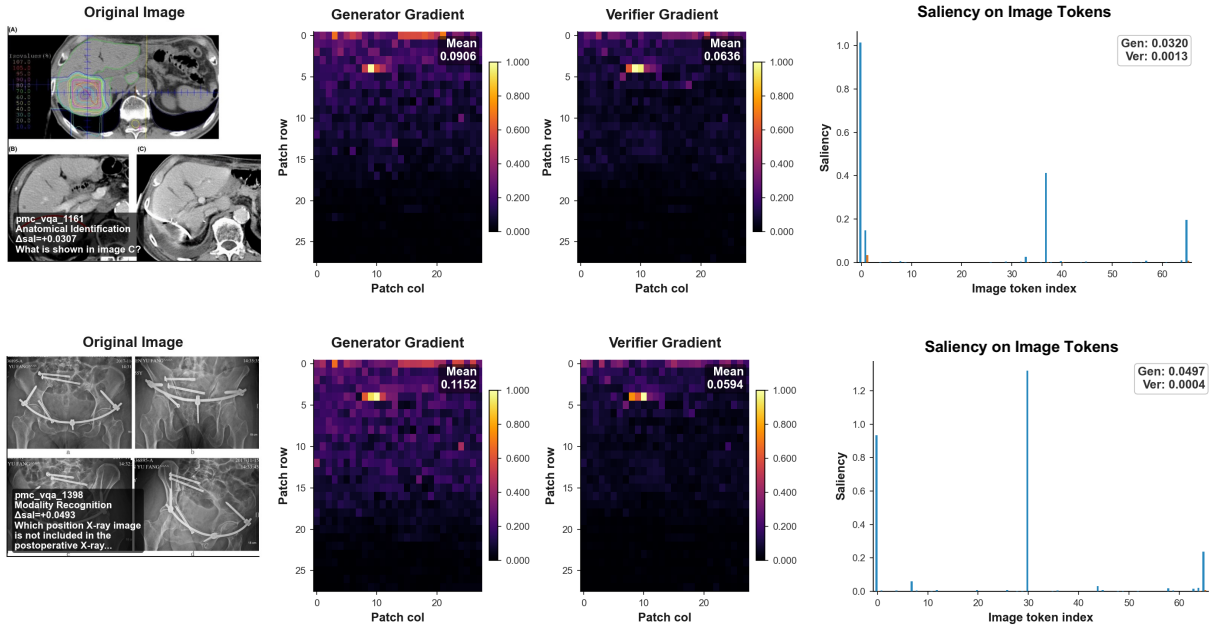


Figure B2 Qualitative evidence of the lazy verifier effect. Compared with the generator, the verifier shows much weaker visual grounding via darker gradient heatmaps and nearly zero image-token saliency. This indicates that the verifier often judges the proposed answer without sufficiently re-grounding in the medical image.

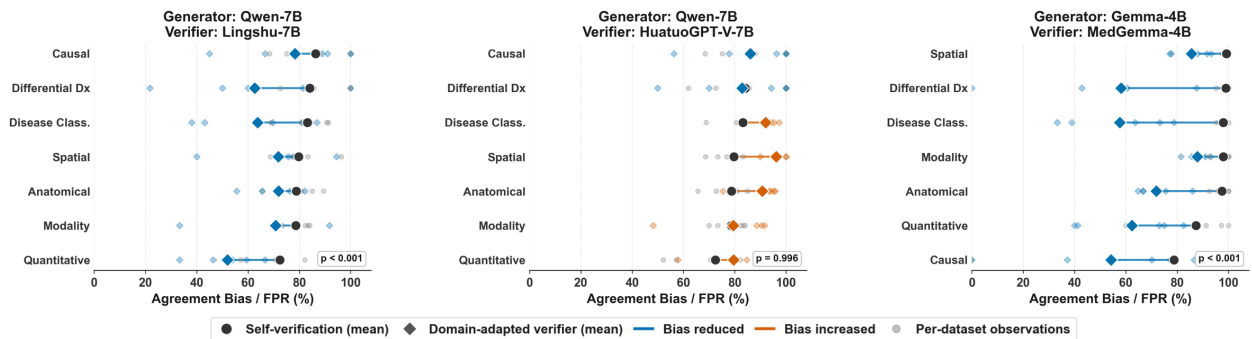


Figure B3 Agreement bias (FPR, %) under self-verification versus a same-size domain-adapted verifier from the related model family. Reasoning types are sorted by self-verification FPR (hardest at top). A filled circle marks self-verification FPR; a diamond marks the domain-adapted verifier FPR; a blue line indicates reduced bias and a red line indicates increased bias. The p -value is from a one-sided Wilcoxon signed-rank test ($H_1: FPR_{\text{self}} > FPR_{\text{domain}}$, $n=35$ pairs per panel).

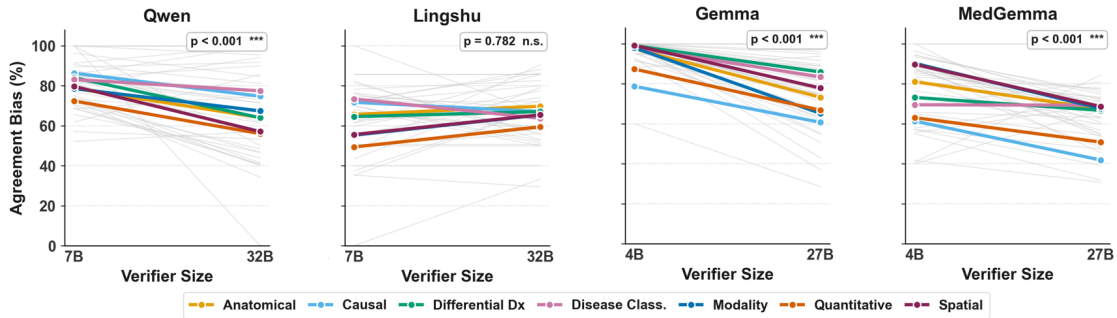


Figure B4 Agreement bias of within-family verifiers across model scales. Each panel corresponds to one model family. Colored lines connect the mean FPR for each medical VQA task, averaged over five datasets; thin gray lines show individual dataset-task paired observations. The p -value in each panel is from a one-sided Wilcoxon signed-rank test (H_1 : the larger verifier has lower FPR than the smaller verifier), pooling all medical VQA tasks and datasets ($n = 35$ pairs per family). Lower FPR indicates less false acceptance.

B.3 Domain-expert Verifier Models Shifts but Does Not Remove Agreement Bias

Figure B3 shows that replacing the self-verifier with a same-size domain-adapted model significantly reduces overall agreement bias in both pairs ($p < 0.001$), yet the blue and red lines reveal that the benefit is highly uneven across reasoning types. Knowledge-intensive types show the largest improvements: in both panels, differential diagnosis and disease classification shift the most to the left (Qwen/Lingshu: -21% and -19% ; Gemma/MedGemma: -41% and -40%). By contrast, spatial reasoning and modality recognition show only modest leftward shifts of 8-14%, remaining above 70% agreement bias even after domain adaptation. Critically, no reasoning type reaches reliable rejection, every diamond in both panels stays above 50%, indicating that domain adaptation shifts the reliability boundary without dissolving it.

B.4 Larger Same-Family Verifiers Reduce False Acceptance Unevenly

We test the *generator-verifier relation boundary*: whether self-verification fails simply because the same model is used for both generation and verification. Figure B4 compares smaller and larger verifiers within the same model family, with colored lines showing mean FPR for each medical VQA task and gray lines showing dataset-level paired observations. Scaling the verifier reduces agreement bias in several families: Qwen, Gemma, and MedGemma all show significant FPR reductions under the paired Wilcoxon test ($p < 0.001$). However, the improvement is not universal. Lingshu shows flat or mixed trends and no significant reduction ($p = 0.782$), indicating that larger related verifiers do not necessarily become better error detectors. The gains are also task-dependent: some tasks improve substantially, while clinically difficult tasks such as disease classification and differential diagnosis remain high-FPR even after scaling. Thus, stronger related verifiers can shift the false-acceptance boundary, but they do not remove it.

B.5 Agreement Bias Accumulates in Multi-Turn Feedback Loops

We provide an additional analysis of the verifier-generator feedback loop to complement Fig. 7 in the main paper. Fig. 7 focuses on the generator’s correctness at turn N compared to turn 0 after repeated verification, while Fig. B5 further shows how agreement bias accumulates over turns and how this accumulation affects the generator’s final performance. Agreement bias increases steadily for all reasoning types, confirming that repeated verification does not improve the system. Instead, the verifier-generator loop increasingly preserves or reinforces incorrect answers. The final generator

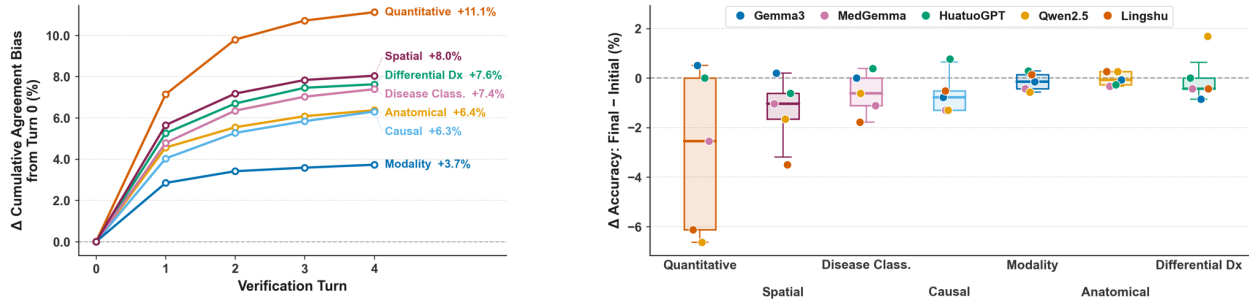


Figure B5 Performance of multi-turn verifier-generator feedback loop. (a) presents the cumulative agreement bias. (b) shows the degraded performance of the generator after five turns. As shown, the degraded performance is roughly proportional to the strength of the agreement bias, as shown on the left.

performance provides an additional downstream view of this failure mode: performance degradation is roughly aligned with the strength of accumulated agreement bias, indicating that false verification is not merely a local verifier error but can propagate into subsequent answer revisions. This result strengthens the conclusion of Fig. 7: once the verifier accepts an incorrect answer, its verdict and explanation can steer later generator turns toward maintaining that answer, turning a single false acceptance into a persistent system-level failure. Therefore, multi-turn self-verification should not be interpreted as a safety mechanism.

C Prompts and Implementation Details

Verifier Below is the prompt we used for the verifier.

You are a medical imaging verification expert. Determine whether the proposed answer to the medical imaging question is CORRECT, INCORRECT, or UNCERTAIN.\n

f"Question: {question}\nProposed Answer: {answer}\n"

"\nRespond in the following format:\nVerdict: [CORRECT or INCORRECT or UNCERTAIN]\nConfidence: [0.0 to 1.0]\nExplanation: [brief justification]\n"

Generator-verifier loop

You are a medical imaging expert. Look at the image carefully and answer the following question concisely.

Question: {question}

Answer:

You are a medical imaging verification expert. Determine whether the proposed answer to the medical imaging question is CORRECT, INCORRECT, or UNCERTAIN.

Question: {question}

Proposed Answer: {answer}

Respond in the following format:

Verdict: [CORRECT or INCORRECT or UNCERTAIN]

Confidence: [0.0 to 1.0]

Explanation: [brief justification]

You are a medical imaging expert. You previously answered a medical imaging question, but a verifier assessed your answer as {verdict.upper()}.

Question: {question}

Your previous answer: {prev_answer}

Verifier's explanation: {explanation}

Please look at the image again carefully, reconsider, and provide a corrected answer.

Answer:

Oracle judge

You are evaluating medical visual question answering outputs. Given the question, the reference answer, and the model answer, decide whether the model answer should be counted as correct.

Rules:

Return CORRECT only if the model answer semantically matches the reference answer.

```

Be strict for yes/no questions.
Accept clear synonyms or equivalent medical phrasing.
No partial credit.
Return only CORRECT or INCORRECT.

f"Question: {question}\nReference Answer: {reference_answer}\nModel Answer:
{model_answer}\n"

```

D Statistical Tests Details

D.1 Logistic GLMM for Generator-Verifier Error Coupling

Objective. The goal of this analysis is to quantify how strongly a verifier’s likelihood of being incorrect is driven by the generator’s correctness, and to test whether this relationship changes across task types, models, and datasets. We perform this analysis at the sample level (each query example), hence both outcomes are binary. We define $\text{gen_err}_i \in \{0, 1\}$ for observation i , where 0 indicates the generator answered correctly and 1 indicates the generator answered incorrectly. Similarly, $\text{ver_err}_i \in \{0, 1\}$ encodes 0 for a correct verifier judgment and 1 for an incorrect one. The quantity of interest is therefore $P(\text{ver_err} = 1 | \text{gen_err})$: the probability that the verifier errs, as a function of whether the generator erred.

Why a logistic model (not linear)? Because the response variable ver_err is binary, a linear model would produce predicted probabilities outside $[0, 1]$ and would impose structurally incorrect homoskedastic residuals (since $\text{Var}(Y) = p(1 - p)$ for a Bernoulli outcome, which is heteroskedastic by definition). We therefore use a *logistic* link function, modelling the log-odds of the verifier being incorrect:

$$\log \frac{P(\text{ver_err}_i = 1)}{P(\text{ver_err}_i = 0)} = \eta_i, \tag{1}$$

where η_i is the linear predictor described below. The natural interpretation of model parameters as *odds ratios* ($\text{OR} = e^\beta$) is also more meaningful for binary data than regression coefficients on a probability scale.

Why mixed effects (not fixed effects only)? The data have a natural grouped structure: observations are nested within (model, dataset, reasoning type) combinations. Treating these groups as pure fixed effects would consume many degrees of freedom and, more importantly, would not allow us to make inferences about the *population* of reasoning types and datasets beyond those observed. A *mixed-effects* model instead treats group-level deviations as draws from a distribution, enabling inference about the variance of the coupling across groups rather than just its value within each group.

Why random slopes (not random intercepts only)? A model with only random intercepts allows each group to have a different *baseline* verifier error rate but constrains the *effect of gen_err* to be identical everywhere. Our research question is precisely whether this effect varies, *i.e.* whether some reasoning types or datasets show a weaker or stronger coupling than others. Answering this requires *random slopes*: allowing each group to have its own gen_err coefficient. The variance of these random slopes, σ_{slope}^2 , directly quantifies how much the coupling fluctuates across groups.

Model specification. We fit three nested models using maximum likelihood (ML) to enable likelihood-ratio testing of fixed effects:

- **M0** (null): random intercepts only, no `gen_err`:

$$\eta_i = \mu + u_{rt[i]} + u_{model[i]} + u_{ds[i]}, \quad (2)$$

where $u_g \sim \mathcal{N}(0, \sigma_g^2)$ for each grouping factor g .

- **M1**: fixed `gen_err` effect, random intercepts only:

$$\eta_i = \beta_0 + \beta_1 \text{gen_err}_i + u_{rt[i]} + u_{model[i]} + u_{ds[i]}. \quad (3)$$

- **M2** (full model): fixed `gen_err` effect, random intercepts *and* random slopes for all three grouping factors:

$$\begin{aligned} \eta_i = & \beta_0 + \beta_1 \text{gen_err}_i + (u_{0,rt[i]} + u_{1,rt[i]} \text{gen_err}_i) \\ & + (u_{0,model[i]} + u_{1,model[i]} \text{gen_err}_i) + (u_{0,ds[i]} + u_{1,ds[i]} \text{gen_err}_i), \end{aligned} \quad (4)$$

where $(u_{0,g}, u_{1,g})^\top \sim \mathcal{N}(\mathbf{0}, \Sigma_g)$ for each grouping factor $g \in \{\text{reasoning type, model, dataset}\}$, and Σ_g is a 2×2 covariance matrix estimating the variance of the intercept deviation, the variance of the slope deviation, and their covariance within group g .

In `lme4` notation (Bates et al., 2015), M2 is written as:

$$\begin{aligned} \text{ver_err} \sim & \text{gen_err} + (1 + \text{gen_err} \mid \text{reasoning_type}) + (1 + \text{gen_err} \mid \text{model}) \\ & + (1 + \text{gen_err} \mid \text{dataset}) \end{aligned}$$

with `family = binomial`.

Model comparison and hypothesis tests. We use likelihood-ratio tests (LRT) to answer two questions:

1. **Does `gen_err` predict `ver_err` at all?** Compare M0 vs. M1. The test statistic $\Lambda = -2(\ell_{M0} - \ell_{M1})$ follows a χ_1^2 distribution under the null hypothesis $\beta_1 = 0$. Result: $\chi_1^2 = 13,577.5$, $p \approx 0$.
2. **Does the coupling vary across groups?** Compare M1 vs. M2. Adding random slopes for three groups introduces 6 additional parameters (one slope variance and one intercept-slope covariance per group), so the test statistic follows χ_6^2 under the null hypothesis $\sigma_{\text{slope},g}^2 = 0$ for all g . Note: because variances are constrained to be non-negative, this test is conservative; the true p -value is even smaller than reported. Result: $\chi_6^2 = 2,577.0$, $p \approx 0$.

Goodness-of-Fit metrics.

- **Nakagawa-Schielezeth R^2 .** For GLMMs, the marginal and conditional R^2 are computed following:

$$R_{\text{marginal}}^2 = \frac{\sigma_f^2}{\sigma_f^2 + \sigma_r^2 + \sigma_d^2}, \quad (5)$$

$$R_{\text{conditional}}^2 = \frac{\sigma_f^2 + \sigma_r^2}{\sigma_f^2 + \sigma_r^2 + \sigma_d^2}, \quad (6)$$

where $\sigma_f^2 = \text{Var}(\hat{\eta}^{\text{fixed}})$ is the variance of the fixed-effect linear predictor, $\sigma_r^2 = \sum_g \text{tr}(\hat{\Sigma}_g)$ is the total variance attributable to random effects (intercepts and slopes), and $\sigma_d^2 = \pi^2/3$ is the distribution-specific variance for the logit link (Nakagawa and Schielzeth, 2013). R_{marginal}^2 captures the explanatory power of `gen_err` alone; $R_{\text{conditional}}^2$ includes group-level heterogeneity.

- **McFadden pseudo- R^2** . As a complementary scalar summary of fit:

$$R^2_{\text{McFadden}} = 1 - \frac{\ell_{\text{M2}}}{\ell_{\text{M0}}}, \quad (7)$$

where ℓ denotes the log-likelihood. Values above 0.2 are conventionally considered good and above 0.4 excellent for binary outcome models (McFadden, 1972).

Results summary. Key fit statistics for M2: marginal $R^2 = 0.259$, conditional $R^2 = 0.773$, McFadden pseudo- $R^2 = 0.407$. The large gap between marginal and conditional R^2 reflects substantial group-level slope heterogeneity, particularly across models.

Table 1 Fixed-effect estimates from M2 (logistic GLMM with random slopes). OR = odds ratio = $e^{\hat{\beta}}$.

Parameter	$\hat{\beta}$	SE	z	p	OR
Intercept	-2.125	0.463	-4.59	< 0.001	0.12
gen_err	4.050	0.773	5.24	< 0.001	57.4

Table 2 Random-effect variance components from M2. σ_{int}^2 = variance of random intercepts; σ_{slope}^2 = variance of random slopes for **gen_err**; ρ = correlation between intercept and slope deviations.

Grouping factor	σ_{int}^2	σ_{slope}^2	ρ
Reasoning type	0.316	0.485	-0.945
Model	1.582	4.876	-0.967
Dataset	0.048	0.128	-0.877

Table 3 Model fit comparison. df = number of estimated parameters.

Model	df	Log-lik	AIC	BIC
M0 (null, random intercepts)	4	-19,844.1	39,696.2	39,729.1
M1 (fixed gen_err, int. only)	5	-13,055.9	26,121.7	26,163.6
M2 (full, random slopes)	11	-11,767.4	23,556.7	23,648.8

D.2 Linear Mixed Models for Generator–Verifier Agreement Bias

Objective and unit of analysis. The goal of this analysis is to quantify how the generator error rate $p_g = 1 - \text{acc}$ shapes four aggregate verifier metrics—FNR, FPR, Bias, and dSkew—and to obtain a population-average estimate of this effect that accounts for baseline differences across reasoning types, models, and datasets.

We perform this analysis at the *cell level*. Each cell is one (reasoning type, model, dataset) combination, yielding $N = 210$ aggregate observations ($7 \times 6 \times 5$). Within each cell, the four metrics are computed from all query examples belonging to that combination, and p_g is the cell-level generator error rate. Unlike the observation-level GLMM (Appendix D.1), the response variables here are continuous proportions rather than binary outcomes, which motivates a linear rather than logistic model.

Why a linear model (not logistic)? The four metrics (FNR, FPR, Bias, dSkew) are continuous quantities defined as proportions or differences of proportions, taking values in $[-1, 1]$. A logistic link is designed for binary outcomes; applying it to a continuous response would be misspecified. A linear mixed model instead assumes $y_{ijk} \sim \mathcal{N}(\mu_{ijk}, \sigma^2)$, which is appropriate for proportion-valued

outcomes when they are not highly skewed and when the sample sizes within each cell are sufficiently large to justify treating sample proportions as approximately Gaussian—both conditions that hold here.

Why mixed effects (not fixed effects only)? The 210 cells are not exchangeable: cells from the same model share idiosyncratic tendencies (e.g., one model may have a systematically higher baseline FPR), and cells from the same dataset share difficulty characteristics. Treating model and dataset as fixed effects would consume many degrees of freedom and, more importantly, would conflate between-group baseline differences with the p_g slope, inflating its standard error. A mixed-effects model instead treats group-level deviations as draws from a distribution, allowing the fixed-effect slope $\hat{\beta}_1$ to be estimated after partialling out these baseline differences.

Why random intercepts only (not random slopes)? A model with random slopes would allow the effect of p_g to differ across reasoning types, models, and datasets—which is scientifically desirable. However, estimating a random slope variance requires a sufficient number of group levels to observe reliable between-group variation in slopes; the conventional minimum is approximately 10 levels per grouping factor. Here we have only 7 reasoning types, 6 models, and 5 datasets. When random slopes were included (formula: $y \sim p_g + (1+p_g|reasoning_type) + (1+p_g|model) + (1+p_g|dataset)$), all four metrics produced singular fits with slope variances collapsing to exactly zero, confirming that the data do not support random slope estimation at this aggregation level. We therefore use random intercepts only, which absorb between-group heterogeneity in baseline metric levels while yielding a single reliable population-average slope $\hat{\beta}_1$. This contrasts with the observation-level GLMM (Appendix D.1), where $N \approx 32,000$ observations provided sufficient power to estimate random slopes.

Model specification. For each metric $y \in \{\text{FNR}, \text{FPR}, \text{Bias}, \text{dSkew}\}$, we fit:

$$y_{ijk} = \beta_0 + \beta_1 p_{g,ijk} + u_i^{(\text{rt})} + u_j^{(\text{model})} + u_k^{(\text{ds})} + \varepsilon_{ijk}, \quad (8)$$

where i, j, k index reasoning type, model, and dataset respectively;

$$\begin{aligned} u_i^{(\text{rt})} &\sim \mathcal{N}(0, \sigma_{\text{rt}}^2), \\ u_j^{(\text{model})} &\sim \mathcal{N}(0, \sigma_{\text{model}}^2), \\ u_k^{(\text{ds})} &\sim \mathcal{N}(0, \sigma_{\text{ds}}^2), \\ \varepsilon_{ijk} &\sim \mathcal{N}(0, \sigma^2), \end{aligned}$$

and all random effects are assumed mutually independent. In `lme4` notation (Bates et al., 2015), the model is:

$$y \sim p_g + (1 | reasoning_type) + (1 | model) + (1 | dataset)$$

Models are estimated using REML, which yields unbiased variance-component estimates when fixed-effect comparisons across models are not required. The BOBYQA optimizer (Powell et al., 2009) is used with a maximum of 2×10^5 function evaluations. The quantity of interest is $\hat{\beta}_1$, the population-average change in the metric per unit increase in p_g , with inference via the Satterthwaite approximation to degrees of freedom (Satterthwaite, 1946).

Goodness-of-Fit metrics. We report marginal and conditional R^2 following Nakagawa and Schielzeth

(2013):

$$R^2_{\text{marginal}} = \frac{\sigma_f^2}{\sigma_f^2 + \sigma_r^2 + \sigma_e^2}, \quad (9)$$

$$R^2_{\text{conditional}} = \frac{\sigma_f^2 + \sigma_r^2}{\sigma_f^2 + \sigma_r^2 + \sigma_e^2}, \quad (10)$$

where $\sigma_f^2 = \text{Var}(\hat{y}^{\text{fixed}}) = \text{Var}(\hat{\beta}_0 + \hat{\beta}_1 p_g)$ is the variance of the fixed-effect predictions, $\sigma_r^2 = \sigma_{\text{rt}}^2 + \sigma_{\text{model}}^2 + \sigma_{\text{ds}}^2$ is the total random-intercept variance, and $\sigma_e^2 = \sigma^2$ is the residual variance. For a linear mixed model the distribution-specific variance is the residual itself (not $\pi^2/3$ as in the logistic case). R^2_{marginal} captures the explanatory power of p_g alone; $R^2_{\text{conditional}}$ includes the additional variance accounted for by the random intercepts.

Results summary. The large gap between marginal and conditional R^2 for FPR and Bias indicates that, while p_g has a significant average effect, much of the cell-to-cell variation in these metrics is driven by which model and dataset the cell belongs to rather than by the generator error rate alone. For dSkew the marginal R^2 is high (0.58), reflecting the algebraic dependence of dSkew on p_g in its definition.

Table 4 Fixed-effect slope estimates from the four cell-level LMMs. Each row is one metric; $\hat{\beta}_1$ is the population-average change per unit increase in p_g ; 95% CI computed via the Wald approximation.

Metric	$\hat{\beta}_0$	$\hat{\beta}_1$	SE	p	95% CI	Sig.
FNR	0.146	-0.040	0.066	0.544	[-0.169, +0.089]	n.s.
FPR	0.666	+0.215	0.071	0.003	[+0.076, +0.355]	**
Bias	0.490	+0.305	0.112	0.008	[+0.085, +0.524]	**
dSkew	-0.113	+0.917	0.054	< 0.001	[+0.812, +1.023]	***

Table 5 Random-intercept variance components and goodness-of-fit for the four cell-level LMMs. σ_{rt}^2 , σ_{model}^2 , σ_{ds}^2 are the estimated random-intercept variances; σ^2 is the residual variance.

Metric	σ_{rt}^2	σ_{model}^2	σ_{ds}^2	σ^2	$R^2_{\text{marg.}}$	$R^2_{\text{cond.}}$
FNR	0.000	0.006	0.002	0.033	0.002	0.254
FPR	0.001	0.013	0.003	0.047	0.047	0.447
Bias	0.002	0.036	0.012	0.079	0.037	0.482
dSkew	0.002	0.011	0.002	0.025	0.577	0.797

Figure B1 shows the cell-level scatter and fitted LMM lines that underpin the per-task forest summary in Fig. 4 (main paper). The same data are summarized as per-task slopes in the main figure; the scatter here exposes the dispersion across the 210 cells and the model-level coloring that drives the conditional R^2 .

E Full Numeric Results

Table 6 Generator accuracy (%) on MedXpert-QA. Rows are reasoning types; columns are generator models. The final column reports the mean across the six generators.

Reasoning	G3	MG	HG	Q7	LS	P4	Mean
Modality	21.4	21.4	14.3	14.3	14.3	21.4	17.9
Anatomy	23.8	20.5	20.5	21.3	24.6	22.1	22.1
Disease Class.	20.0	26.4	22.6	22.9	24.9	20.0	22.8
Spatial	28.6	9.5	9.5	14.3	0.0	14.3	12.7
Causal	16.6	21.7	19.8	24.9	26.5	19.4	21.5
Diff. Dx.	16.9	24.2	18.5	20.8	24.2	18.0	20.4
Quant.	11.8	23.5	17.6	11.8	5.9	5.9	12.7
Overall	19.4	24.7	21.2	22.6	24.4	19.6	22.0

Table 7 Generator accuracy (%) on PathVQA. Rows are reasoning types; columns are generator models. The final column reports the mean across the six generators.

Reasoning	G3	MG	HG	Q7	LS	P4	Mean
Modality	28.6	34.3	42.9	28.6	34.3	31.4	33.3
Anatomy	45.7	40.0	48.6	42.9	54.3	45.7	46.2
Disease Class.	31.4	31.4	42.9	28.6	51.4	22.9	34.8
Spatial	31.4	31.4	45.7	22.9	54.3	22.9	34.8
Causal	37.1	37.1	34.3	40.0	37.1	37.1	37.1
Diff. Dx.	31.4	45.7	65.7	34.3	80.0	60.0	52.9
Quant.	28.6	31.4	40.0	22.9	51.4	31.4	34.3
Overall	33.5	35.9	45.7	31.4	51.8	35.9	39.0

Table 8 Generator accuracy (%) on PMC-VQA. Rows are reasoning types; columns are generator models. The final column reports the mean across the six generators.

Reasoning	G3	MG	HG	Q7	LS	P4	Mean
Modality	50.5	48.8	58.5	54.6	56.4	44.1	52.2
Anatomy	16.1	18.4	21.3	18.0	17.0	12.4	17.2
Disease Class.	15.6	18.1	24.8	17.9	18.7	14.1	18.2
Spatial	18.1	23.6	35.2	24.2	23.6	15.4	23.4
Causal	21.1	23.7	26.3	21.1	34.2	18.4	24.1
Diff. Dx.	0.0	12.5	12.5	25.0	12.5	0.0	10.4
Quant.	26.0	30.0	28.0	34.0	32.0	24.0	29.0
Overall	24.4	26.2	32.2	27.5	27.8	20.7	26.5

Table 9 Generator accuracy (%) on SLAKE. Rows are reasoning types; columns are generator models. The final column reports the mean across the six generators.

Reasoning	G3	MG	HG	Q7	LS	P4	Mean
Modality	80.3	83.2	92.0	78.1	97.8	81.8	85.5
Anatomy	64.5	70.8	66.6	64.1	82.2	60.6	68.1
Disease Class.	56.5	63.0	50.0	44.2	44.9	23.9	47.1
Spatial	27.6	55.2	52.1	47.2	58.9	41.1	47.0
Causal	24.6	33.3	42.1	50.9	68.4	31.6	41.8
Diff. Dx.	76.9	53.8	53.8	15.4	61.5	61.5	53.8
Quant.	43.7	43.7	54.9	50.7	74.7	50.7	53.1
Overall	56.5	64.9	63.2	58.5	74.3	53.3	61.8

Table 10 Generator accuracy (%) on VQA-RAD. Rows are reasoning types; columns are generator models. The final column reports the mean across the six generators.

Reasoning	G3	MG	HG	Q7	LS	P4	Mean
Modality	61.1	66.7	72.2	72.2	68.5	51.8	65.4
Anatomy	34.0	50.5	63.1	56.3	59.2	43.7	51.1
Disease Class.	50.3	64.6	65.2	57.5	60.8	51.9	58.4
Spatial	46.4	60.7	61.9	46.4	52.4	42.9	51.8
Causal	100.0	100.0	50.0	75.0	25.0	50.0	66.7
Diff. Dx.	0.0	50.0	50.0	0.0	0.0	50.0	25.0
Quant.	26.1	43.5	65.2	69.6	47.8	39.1	48.6
Overall	46.1	60.1	64.7	57.4	58.5	47.7	55.8

Table 11 Verifier results on MedXpert-QA. Each cell reports verification accuracy / false positive rate / false negative rate (%). The final column reports the mean triplet across the six self-verifiers.

Reasoning	G3	MG	HG	Q7	LS	P4	Mean
Modality	21.4	14.3	21.4	21.4	57.1	50.0	31.0
	100.0	100.0	91.7	83.3	50.0	60.0	80.8
	0.0	33.3	0.0	50.0	0.0	33.3	19.4
	29.5	27.9	20.5	44.5	54.1	52.8	38.2
Anatomy	92.5	89.7	96.9	65.6	43.5	42.6	71.8
	0.0	4.0	8.3	19.2	53.3	72.7	26.3
	22.0	31.0	27.4	40.6	42.5	43.1	34.4
	97.0	91.6	93.5	68.8	66.4	62.2	79.9
Disease Class.	1.6	6.2	1.4	27.9	30.4	38.0	17.6
	28.6	19.1	14.3	28.6	52.4	46.2	31.5
	100.0	89.5	94.7	83.3	47.6	45.5	76.8
	0.0	0.0	0.0	0.0	0.0	100.0	16.7
Spatial	17.4	26.9	23.7	36.9	47.0	49.7	33.6
	98.6	89.4	94.1	75.1	62.9	54.7	79.1
	2.4	14.5	4.0	27.0	25.4	33.3	17.8
	20.8	34.3	21.3	35.8	45.5	39.8	32.9
Diff. Dx.	95.3	83.0	94.5	72.7	61.5	59.6	77.7
	0.0	11.6	9.1	32.4	32.6	62.5	24.7
	43.8	62.5	29.4	50.0	64.7	66.7	52.8
	60.0	41.7	78.6	57.1	37.5	37.5	52.1
Quant.	0.0	25.0	33.3	0.0	0.0	0.0	9.7
	22.0	30.5	25.4	39.6	45.0	44.9	34.6
Overall	96.4	89.7	93.8	70.2	62.8	58.7	78.6
	1.3	8.3	3.5	27.1	30.6	43.1	19.0

Table 12 Verifier results on PathVQA. Each cell reports verification accuracy / false positive rate / false negative rate (%). The final column reports the mean triplet across the six self-verifiers.

Reasoning	G3	MG	HG	Q7	LS	P4	Mean
Modality	28.6	26.5	45.7	34.3	42.9	34.3	35.4
	100.0	86.4	100.0	84.0	78.3	95.8	90.7
	0.0	50.0	0.0	20.0	16.7	0.0	14.4
Anatomy	47.1	65.6	51.4	47.1	57.1	51.6	53.3
	100.0	57.9	94.4	89.5	75.0	87.5	84.0
	0.0	0.0	0.0	6.7	15.8	6.7	4.9
Disease Class.	37.5	45.2	47.1	30.3	40.0	31.0	38.5
	95.2	65.0	100.0	91.3	82.3	81.8	86.0
	0.0	36.4	0.0	20.0	38.9	28.6	20.6
Spatial	31.4	36.4	48.6	25.7	65.7	45.5	42.2
	100.0	90.9	100.0	96.3	50.0	72.0	84.9
	0.0	9.1	0.0	0.0	21.1	0.0	5.0
Causal	39.4	48.5	34.3	54.5	42.9	45.5	44.2
	95.2	55.0	95.7	68.4	68.2	85.0	77.9
	0.0	46.2	8.3	14.3	38.5	7.7	19.2
Diff. Dx.	37.0	33.3	67.7	60.6	54.3	67.7	53.4
	100.0	57.1	100.0	61.9	85.7	90.9	82.6
	0.0	75.0	0.0	0.0	35.7	0.0	18.5
Quant.	36.4	50.0	52.9	51.6	54.3	48.0	48.9
	91.3	57.1	76.2	52.2	35.3	72.2	64.1
	0.0	36.4	0.0	37.5	55.6	0.0	21.6
	36.8	43.6	49.7	43.4	51.0	46.2	45.1
Overall	97.4	67.1	95.2	77.7	67.8	83.6	81.5
	0.0	36.1	1.2	14.1	31.7	6.1	14.9

Table 13 Verifier results on PMC-VQA. Each cell reports verification accuracy / false positive rate / false negative rate (%). The final column reports the mean triplet across the six self-verifiers.

Reasoning	G3	MG	HG	Q7	LS	P4	Mean
Modality	51.8	50.1	60.7	57.8	63.5	56.7	56.8
	97.4	94.5	94.8	82.3	71.8	78.5	86.5
	0.0	3.1	0.4	9.1	9.2	7.3	4.8
Anatomy	17.0	22.4	23.5	29.5	45.9	39.3	29.6
	98.8	93.4	96.9	85.0	61.7	66.6	83.7
	0.0	7.6	3.0	5.7	17.3	24.6	9.7
Disease Class.	16.6	31.1	26.2	24.6	36.0	38.4	28.8
	99.0	81.1	98.0	90.6	72.5	66.3	84.6
	0.0	12.9	1.7	5.9	27.0	25.9	12.2
Spatial	19.3	26.4	37.0	35.2	48.4	49.4	35.9
	98.7	94.2	96.6	76.9	59.7	60.3	81.1
	0.0	7.0	1.6	26.2	25.6	16.7	12.8
Causal	19.4	27.0	28.9	18.9	44.7	41.7	30.1
	100.0	96.4	93.1	100.0	72.0	72.2	89.0
	12.5	0.0	0.0	12.5	23.1	16.7	10.8
Diff. Dx.	0.0	25.0	25.0	25.0	20.0	20.0	20.0
	100.0	85.7	85.7	100.0	85.7	80.0	89.5
	0.0	0.0	0.0	0.0	0.0	0.0	0.0
Quant.	26.5	42.9	31.2	32.6	60.0	35.3	38.1
	97.2	73.5	97.1	82.1	35.3	73.3	76.4
	7.7	20.0	0.0	40.0	50.0	0.0	19.6
	25.4	31.9	34.3	35.3	48.1	43.9	36.5
Overall	98.5	90.4	96.5	85.2	66.1	69.0	84.3
	0.4	7.9	1.8	9.4	19.3	19.3	9.7

Table 14 Verifier results on SLAKE. Each cell reports verification accuracy / false positive rate / false negative rate (%). The final column reports the mean triplet across the six self-verifiers.

Reasoning	G3	MG	HG	Q7	LS	P4	Mean
Modality	81.0	75.9	91.2	83.2	100.0	89.3	86.8
	92.6	87.0	63.6	70.0	0.0	84.6	66.3
	0.9	11.4	4.0	1.9	0.0	1.0	3.2
Anatomy	65.9	65.8	70.8	70.7	82.2	70.2	70.9
	95.9	87.8	83.2	72.8	81.4	75.7	82.8
	0.0	12.3	2.2	5.5	4.0	5.0	4.8
Disease Class.	57.5	52.7	55.8	55.5	56.5	44.1	53.7
	100.0	40.9	91.1	80.6	69.7	85.0	77.9
	0.0	50.6	3.1	4.9	11.3	14.3	14.0
Spatial	29.4	54.6	46.6	57.0	63.2	55.3	51.0
	97.5	89.0	97.5	68.7	50.7	72.0	79.2
	0.0	10.0	10.8	14.7	27.1	13.6	12.7
Causal	23.6	51.8	42.3	50.0	71.9	34.0	45.6
	100.0	65.8	93.5	88.0	55.6	96.9	83.3
	0.0	11.1	4.8	14.8	15.4	0.0	7.7
Diff. Dx.	83.3	83.3	54.5	33.3	69.2	16.7	56.7
	100.0	40.0	100.0	85.7	40.0	75.0	73.5
	0.0	0.0	14.3	0.0	25.0	100.0	23.2
Quant.	43.7	45.1	59.2	61.4	74.7	63.3	57.9
	100.0	87.5	78.1	70.6	72.2	65.0	78.9
	0.0	12.9	10.3	8.3	9.4	17.2	9.7
	57.6	61.8	65.2	66.0	77.0	63.9	65.3
Overall	96.8	80.0	84.3	73.6	62.2	77.9	79.1
	0.1	16.6	4.7	7.0	9.2	8.7	7.7

Table 15 Verifier results on VQA-RAD. Each cell reports verification accuracy / false positive rate / false negative rate (%). The final column reports the mean triplet across the six self-verifiers.

Reasoning	G3	MG	HG	Q7	LS	P4	Mean
Modality	58.5	66.7	66.7	75.9	75.9	56.5	66.7
	100.0	83.3	93.3	73.3	76.5	95.2	86.9
	3.1	8.3	10.3	5.1	0.0	0.0	4.5
Anatomy	35.0	56.3	61.2	56.0	68.9	58.8	56.0
	100.0	76.5	92.7	81.0	66.7	65.7	80.4
	0.0	11.5	3.2	17.2	6.6	15.2	9.0
Disease Class.	50.0	60.7	66.8	61.7	61.9	55.4	59.4
	98.8	68.8	93.8	84.5	76.1	90.0	85.3
	1.2	23.9	0.0	6.7	13.6	9.6	9.2
Spatial	47.0	60.7	60.7	51.2	54.8	65.7	56.7
	100.0	84.9	100.0	73.3	70.0	57.9	81.0
	0.0	9.8	1.9	20.5	22.7	6.2	10.2
Causal	100.0	100.0	50.0	75.0	25.0	50.0	66.7
	0.0	0.0	100.0	100.0	100.0	100.0	66.7
	0.0	0.0	0.0	0.0	0.0	0.0	0.0
Diff. Dx.	0.0	50.0	50.0	0.0	50.0	0.0	25.0
	100.0	100.0	100.0	100.0	50.0	100.0	91.7
	0.0	0.0	0.0	0.0	0.0	0.0	0.0
Quant.	34.8	68.4	68.2	52.4	60.9	45.5	55.0
	88.2	55.6	87.5	100.0	66.7	100.0	83.0
	0.0	10.0	0.0	26.7	9.1	16.7	10.4
	46.5	61.1	64.2	59.5	63.4	57.4	58.7
Overall	98.0	74.2	94.4	81.3	72.5	79.7	83.3
	0.8	15.6	2.3	12.4	11.7	9.3	8.7

Practical implications. Our verification feasibility map provides actionable guidance for deploying VLMs in clinical settings. For perceptual tasks (modality recognition, anatomical identification), lightweight self-verification is sufficient. For knowledge-intensive tasks (differential diagnosis, causal reasoning), self-verification should not be trusted; instead, systems should integrate external knowledge sources such as clinical guidelines, knowledge graphs, or retrieval-augmented verification. The map can be used as a decision function: given a question, classify its reasoning type, look up the feasibility score, and route to the appropriate verification mode.

Declaration of LLM Usage. The authors used large language models (LLMs) solely for writing assistance, including grammar correction, wording refinement, formatting support, and improving the clarity of the manuscript. The LLMs were not used to generate scientific ideas, design experiments, conduct analyses, produce results, create figures or tables, or draw conclusions. All technical content, methodology, experiments, interpretations, and final claims were developed, verified, and approved by the authors.

Broader Impact. This work aims to support safer use of vision-language models in medical settings by identifying when self-verification can produce false confidence rather than reliable error detection. Our findings caution against using self-verification as a standalone safety mechanism, especially for clinically consequential reasoning tasks. The proposed analysis is intended for risk assessment and model evaluation, not autonomous clinical deployment. Any real-world use of medical VLMs should require rigorous validation, regulatory review, and human expert oversight.